Non-Invasive Characterization of Atrio-Ventricular Properties During Atrial Fibrillation

Mattias Karlsson[1,2], Mikael Wallman[1], Sara R. Ulimoen[3], Frida Sandberg[2]

[1] Dept. of Systems and Data Analysis, Fraunhofer-Chalmers Centre, Gothenburg, Sweden
[2] Dept. of Biomedical Engineering, Lund University, Lund, Sweden
[3] Vestre Viken Hospital Trust, Bærum Hospital, Rud, Norway

Abstract

The atrio-ventricular (AV) node is the primary regulator of ventricular rhythm during atrial fibrillation (AF). Hence, ECG based characterization of AV node properties can be an important tool for monitoring and predicting the effect of rate control drugs. In this work we present a network model of the AV node, and an associated workflow for robust estimation of the model parameters from ECG.

The model consists of interacting nodes with refractory periods and conduction delays determined by the stimulation history of each node. The nodes are organized in one fast pathway (FP) and one slow pathway (SP), interconnected at their last nodes. Model parameters are estimated using a genetic algorithm with a fitness function based on the Poincaré plot of the RR interval series.

The robustness of the parameter estimates was evaluated using simulated data based on ECG measurements. Results from this show that refractory period parameters R_{min}^{SP} and ΔR^{SP} can be estimated with an error (mean $\pm$ std) of 10$\pm$22 ms and -12.6$\pm$26 ms respectively, and conduction delay parameters $D_{min,tot}^{SP}$ and ΔD_{tot}^{SP} with an error of 7$\pm$35 ms and 4$\pm$36 ms. Corresponding results for the fast pathway are 31.7$\pm$65 ms, -0.3$\pm$77 ms, and 17$\pm$29 ms, 43$\pm$109 ms. This suggest that AV node properties can be assessed from ECG during AF with enough precision and robustness for monitoring the effect of rate control drugs.

1. Introduction

It is estimated that 2-4% of the adult population suffers from atrial fibrillation (AF), making it the most common cardiac arrhythmia [1]. It is characterized by rapid and disorganized beating of the atria, leading to rapid and irregular heart rate. Rate control drugs, mainly beta-blockers and calcium channel blockers, are used to lower heart rate by modulating the conduction through the atrioventricular (AV) node [1]. Currently, the choice of drug is largely based on trial and error. Thus, a method for characterization of the AV node on a patient specific level during AF could be beneficial to achieve optimal rate control.

The AV node acts as a gatekeeper between the atria and ventricles and can block or delay incoming impulses. Functionally, it consists of the slow pathway (SP) and the fast pathway (FP), with the FP conducting impulses faster than the SP but with a longer refractory period [2]. The pathways are connected before entering the bundle of His. During AF, when the beating of the atria is rapid and disorganized, conduction through the AV node is thought to alternate between SP and FP.

Mathematical models have become an important tool for understanding and modeling of the impulse blocking and delay in the AV node. Several models of the human AV node have been proposed [3–5]. However, these models have not been developed to be used with exclusively non-invasive measurements, which is important in clinical setting. One exception is the statistical model presented in [6]. This model was developed for estimation of AV node parameters from surface electrocardiogram (ECG) data during AF and is able to replicate patient RR histograms. However, in that model the conduction delay and refractory period are lumped together, making the estimated parameters difficult to interpret.

In this work, we present a model of the AV node with parameters quantifying conduction delay and refractory period. Furthermore, we also present a workflow for parameter estimation from ECG data consisting of a fitness function based on the Poincaré plot together with a problem specific genetic algorithm (GA). A more detailed version of this work can be found at [7].

2. Network Model of the AV Node

The model of the AV node consists of a network of nodes, based on the model presented in [8]. The model comprises two pathways connected to the ventricles via a coupling node denoted the His and Purkinje (HP) node, as seen in Figure 1. Each node corresponds to a localized part of the AV node, and each pathway is modeled with 10

nodes. All nodes can block or delay incoming impulses, and all but the HP node transmit impulses to adjacent nodes, whereas the HP node only receives impulses. For each incoming impulse (n) to the node (i), a refractory period $(R_i(n))$, which controls the blocking, and a conduction delay $(D_i(n))$, which controls the delay are calculated. Both $R_i(n)$ and $D_i(n)$ are dependent on the stimulation history of the node, as described in Equations 1, 2, and 3.

$$R_i(n) = R_{min} + \Delta R(1 - e^{-\tilde{t}_i(n)/\tau_R}) \quad (1)$$

$$D_i(n) = D_{min} + \Delta D e^{-\tilde{t}_i(n)/\tau_D} \quad (2)$$

$$\tilde{t}_i(n) = t_i(n) - t_i(n-1) - R_i(n-1) \quad (3)$$

Here $\tilde{t}_i(n)$ refers to diastolic interval preceding impulse n, and $t_i(n)$ the arrival time of impulse n at node i. When $\tilde{t}_i(n)$ is negative, the node is in its refractory period and the impulse is blocked. Hence, the refractory period and conduction delay are defined by three parameters each, the minimum value, R_{min} and D_{min}; the maximum prolongation, ΔR and ΔD; and the time constants τ_R and τ_D. Each parameter is assumed to be identical for the nodes in the SP and FP, respectively.

The HP node models the connection between the AV node and the bundle of His, the bundle of His, and the Purkinje fibers. Similar to the other nodes, it has a refractory period and a conduction delay. However, in contrast to the SP and FP nodes, these values are set to constants. The refractory period for the HP node is estimated, based on simulations of the model, as the mean of the ten shortest RR intervals, RR_{min}. The conduction delay for the HP node is set to 60 ms based on clinical studies [9].

This results in 12 free parameters for the proposed model, namely $[R_{min}^{FP}, \Delta R^{FP}, \tau_R^{FP}, R_{min}^{SP}, \Delta R^{SP}, \tau_R^{SP}, D_{min}^{FP}, \Delta D^{FP}, \tau_D^{FP}, D_{min}^{SP}, \Delta D^{SP}, \tau_D^{SP}]$. The first node of each pathway is simultaneously stimulated for incoming impulses from the atria. The impulse propagation through the model is then computed using a modified version of Dijkstra's algorithm [8]. The total minimum conduction delay and maximum prolongation, defined as $D_{min,tot}^{FP} = N_n D_{min}^{FP}$; $\Delta D_{tot}^{FP} = N_n \Delta D^{FP}$; $D_{min,tot}^{SP} = N_n D_{min}^{SP}$; $\Delta D_{tot}^{SP} = N_n \Delta D^{SP}$; where $N_n = 10$ are the number of nodes in each

pathway, are introduced for convenience of presentation. The code for the model together with an user example can be found at `https://github.com/FraunhoferChalmersCentre/AV-node-model`.

3. Model parameter estimation

As seen from Figure 1, the input to the model is a series of atrial impulse arrival times. This is modeled by a Poisson process with mean arrival rate λ estimated from the f-waves in the ECG after spatiotemporal QRST cancellation [10] [11]. The output of the model is an RR interval series. This modeled RR interval series is compared to an RR interval series extracted from ECG data, and the similarity is quantified by a fitness function. In order to take the dynamics of the RR interval series into account, the fitness function is based on the Poincaré plot, i.e., a scatter plot of successive pairs of RR intervals. The RR interval series extracted from the ECG and the model output are binned into two dimensional bins centered between 250 ms and 1800 ms in steps of 50 ms, resulting in $N = 961$ bins. The error function is computed according to Equation 4.

$$\epsilon = \frac{1}{N} \sum_{i=1}^{N} \left((x_i - \tilde{x}_i)^2 / \sqrt{\tilde{x}_i} \right) \quad (4)$$

Here x_i and $\tilde{x}_i$ are the number of RR intervals in the i-th bin for the modeled and extracted RR interval series, respectively. The normalization by $\sqrt{\tilde{x}_i}$ is introduced in order to avoid that bins with a large number of data points dominate the optimization, while at the same time avoiding that bins with small number of data points have the same influence on the error.

3.1. Genetic algorithm

A two-stage GA approach is used to minimize ϵ. The first stage aims to get a broad search of the parameter space in order to reduce the risk of premature convergence whereas the second stage aims to find the best fit. The first stage consists of five separate GA and was implemented by restarting the algorithm five times with 300 individuals in each generation, which lasted for six generations. For each
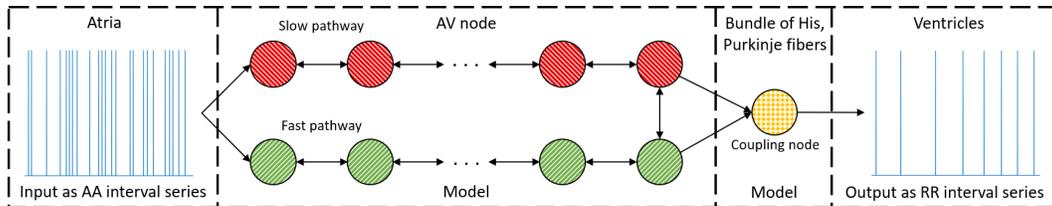

Figure 1: A schematic representation of the proposed model. Arrows indicates the allowed conduction direction and the colors represent nodes with the same parameter sets. Only a subset of the ten nodes in each pathway are showed.

of these restarts the individuals were initialized using a latin hypercube sampling in the ranges; $\{R_{min}^{SP}, R_{min}^{FP}\} \in [250, 600]\ ms$; $\{\Delta R^{SP}, \Delta R^{FP}\} \in [0, 600]\ ms$, $\{\tau_R^{SP}, \tau_R^{FP}\} \in [50, 300]\ ms$; $\{D_{min}^{SP}, D_{min}^{FP}\} \in [0, 30]\ ms$; $\{\Delta D^{SP}, \Delta D^{FP}\} \in [0, 75]\ ms$; $\{\tau_D^{SP}, \tau_D^{FP}\} \in [50, 300]\ ms$. The 150 fittest individuals for each restart were then saved and used as input to the second stage. Hence, the second stage uses a population of 750 individuals in each generation. For both stages, the next generation individuals are created via tournament selection, two-point crossover, and creep mutation [12]; apart from the 2.5% fittest individuals, which survive into the next generation unchanged. During crossover, mating restrictions between too similar individuals were implemented, as well as a varying mutation rate depending on the populations diversity [12]. The termination for the second stage occurs either when 15 generations have been run, or when the ϵ for the fittest individual in each generation does not change for three generations.

Due to the stochastic nature of the Poisson process, ϵ changes between realizations. The magnitude of this variation depends on the model's resulting RR interval series length L_{RR}, where longer L_{RR} reduces the variation in ϵ. However, the running time for the model is linearly dependent on L_{RR}. The variation relative to ϵ is smaller for larger ϵ, i.e., early in the optimization. Thus, L_{RR} is increased throughout the optimization to find a good balance between computer complexity and optimal estimations. This is implemented by changing L_{RR} gradually between generations; with L_{RR} as 1000 for the first stage, as 3000 for the five first generations of the second stage, as 5000 for the following five generations, as 7500 for the next three, and ending with 10000 for the last two.

4. Results

All ECG data used for the evaluations were 15 minutes long ECG segment from the RATe control in Atrial Fibrillation study [13]. Simulated data based on RR interval series from five patients were used to evaluate the robustness of the parameter estimation. These simulated data sets were created by first optimizing the parameters to fit to RR interval series extracted from ECG measurements from the five selected patients, before using the resulting parameters to simulate RR interval series. The λ used for the five simulated data sets were set to the estimated λ from the ECG which the simulation was based upon.

The model and associated workflow were then used to estimate parameters replicating the simulated RR interval series 200 times, and the results are listed in Table 1. The mean error is defined as the difference between the value of the estimated parameter and the ground truth, averaged over the five simulated data sets. The normalized error is also listed, where the normalization is with respect to the parameter ranges, cf. Sec 3.1. One example of the modeled RR interval series compared to the measured can be seen in Figure 3, where both the histogram and Poincaré plot are shown. Moreover, the average percentage of impulses conducted via the SP for the five simulated data sets were [54, 60, 85, 77, 92]%. It is evident from this that the SP is the most dominant pathway for all simulations.

To set the robustness in perspective and to verify that the methodology is applicable to measured data, the parameters were estimated 200 times for a single patient during both baseline and under the influence of the rate control drug Diltiazem, seen in Figure 2. These results indicate that the variation in parameter estimation is lower than the drug effect.

Table 1: Mean error $\pm$ std and normalized error $\pm$ std for each parameter, averaged over the five data sets.

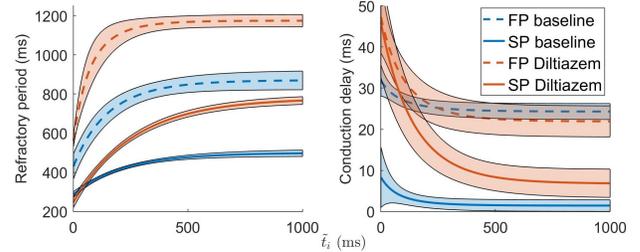| Parameter (ms)	Error (ms)	Normalized error (%)
R_{min}^{FP}	31.7 ± 65	7.9 ± 16
ΔR^{FP}	-0.3 ± 77	-0.1 ± 12
τ_R^{FP}	9.4 ± 45	3.6 ± 17
R_{min}^{SP}	10.3 ± 22	2.6 ± 6
ΔR^{SP}	-12.6 ± 26	-1.9 ± 4
τ_R^{SP}	2.2 ± 32	0.8 ± 12
$D_{min,tot}^{FP}$	17 ± 29	5.7 ± 10
ΔD_{tot}^{FP}	43 ± 109	5.7 ± 15
τ_D^{FP}	17 ± 46	7.1 ± 19
$D_{min,tot}^{SP}$	7 ± 35	2.5 ± 12
ΔD_{tot}^{SP}	4 ± 36	0.5 ± 5
τ_D^{SP}	29 ± 43	12 ± 18

Figure 2: The mean (line) $\pm$ std (shaded background) of the estimated refractory periods and conduction delays, cf. Equations 1-2, for the FP (dashed) and the SP (solid) from one patient at baseline (blue) and during treatment with Diltiazem (orange), respectively.

5. Discussion

A mathematical model of the AV node taking the bundle of His and Purkinje fibers into account, along with a fitness function accounting for RR interval dynamics and a genetic algorithm tailored to the model have been presented. The methodology's robustness and accuracy have been evaluated with simulated and measured data.
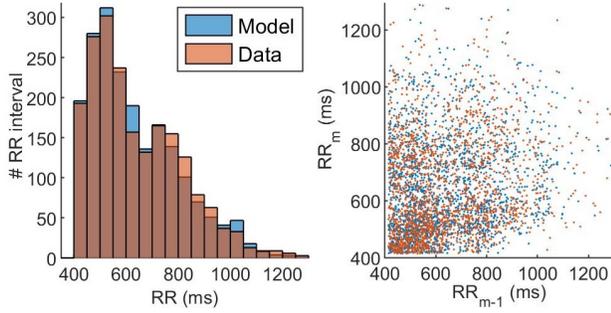
Figure 3: Histogram (left) and Poincaré plot (right) of the modeled (blue) and the measured (orange) RR interval series.

It can be seen from the errors in Table 1 that the parameters associated to the SP are all estimated with an error lower than 30 ms and a std below 50 ms. The parameters for the FP are less robustly estimated, likely due to SP being the dominant pathway. However, with the lower ratio of impulses conducting through it, it has a smaller effect on the result. From the normalized error it is possible to see that the time constants τ_R^{FP}, τ_R^{SP}, τ_D^{FP}, and τ_D^{SP} are less robustly estimated, suggesting lower impact on the output RR interval series.

The good match between modeled and measured RR interval series seen in Figure 3 indicates that the model can represent not only the histogram, but also the dynamics in the Poincaré plot.

Furthermore, the estimates on measured data shown in Figure 2 suggest that it is possible to assess the effect of rate control drugs on both the refractory period and the conduction delay of the AV node from ECG measurements, which can be useful in both drug development and personalized treatment.

Much emphasis has been placed on the robustness of the parameter estimates, since it is important that the parameters are robustly estimated if the they are to be used as bio-markers for treatment prediction and in turn assist in treatment selection.

A natural next step is the analysis of more and longer measurements, as well as several different rate control drugs, to further investigate the applicability of the presented methodology to characterizing the effects of rate control drugs.

6.   Conclusion

We have presented a network model of the AV node taking the bundle of His and Purkinje fibers into account. The model and associated workflow has been shown able to robustly estimate both refractory period and conduction delay in the AV node during AF from non-invasive data, making it possible to asses drug effects on the AV node.

References

[1] Hindricks G, et al. 2020 ESC guidelines for the diagnosis and management of atrial fibrillation developed in collaboration with the european association of cardio-thoracic surgery (EACTS). EUR HEART J 2020;.

[2] Kurian T, Ambrosi C, Hucker W, Fedorov VV, Efimov IR. Anatomy and electrophysiology of the human AV node. PACE 2010;33(6):754–762.

[3] Lian J, Mussig D, Lang V. Computer modeling of ventricular rhythm during atrial fibrillation and ventricular pacing. IEEE T BIO MED ENG 2006;53(8):1512–1520.

[4] Inada S, Hancox J, Zhang H, Boyett M. One-dimensional mathematical model of the atrioventricular node including atrio-nodal, nodal, and nodal-his cells. Biophys J 2009; 97(8):2117–2127.

[5] Climent AM, Guillem MS, Zhang Y, Millet J, Mazgalev T. Functional mathematical model of dual pathway AV nodal conduction. AM J PHYSIOL HEART C 2011; 300(4):H1393–H1401.

[6] Corino VD, Sandberg F, Mainardi LT, Sornmo L. An atrioventricular node model for analysis of the ventricular response during atrial fibrillation. IEEE T BIO MED ENG 2011;58(12):3386–3395.

[7] Karlsson M, Sandberg F, Ulimoen SR, Wallman M. Non-invasive characterization of human AV-nodal conduction delay and refractory period during atrial fibrillation. FRONT PHYSIOL 2021;.

[8] Wallman M, Sandberg F. Characterisation of human AV-nodal properties using a network model. MED BIOL ENG COMPUT 2018;56(2):247–259.

[9] Deshmukh P, Casavant DA, Romanyshyn M, Anderson K. Permanent, direct his-bundle pacing: a novel approach to cardiac pacing in patients with normal his-purkinje activation. Circulation 2000;101(8):869–877.

[10] Stridh M, Sornmo L. Spatiotemporal qrst cancellation techniques for analysis of atrial fibrillation. IEEE T BIO MED ENG 2001;48(1):105–111.

[11] Corino VD, Sandberg F, Lombardi F, Mainardi LT, Sörnmo L. Atrioventricular nodal function during atrial fibrillation: Model building and robust estimation. BIOMED SIGNAL PROCES 2013;8(6):1017–1025.

[12] Wahde M. Biologically inspired optimization methods: an introduction. WIT press, 2008.

[13] Ulimoen SR, Enger S, Carlson J, Platonov PG, Pripp AH, Abdelnoor M, Arnesen H, Gjesdal K, Tveit A. Comparison of four single-drug regimens on ventricular rate and arrhythmia-related symptoms in patients with permanent atrial fibrillation. Am J Cardiol 2013;111(2):225–230.

Address for correspondence:

Mattias Karlsson
Chalmers Science Park SE-412 88 Göteborg, Sweden
Mattias.karlsson@fcc.chalmers.se